

High efficiency flexible ITO-free polymer/fullerene photodiodes

J. Huang,^a X. Wang,^a Y. Kim,^a A. J. deMello,^b D. D. C. Bradley^{*a} and J. C. deMello^{*b}

Received 17th May 2006, Accepted 9th June 2006

First published as an Advance Article on the web 23rd June 2006

DOI: 10.1039/b607016g

We report efficient polymer photodiodes fabricated on flexible polyethyleneterephthalate (PET) substrates. The PET substrates were coated with a layer of poly(3,4-ethylene-dioxythiophene): polystyrenesulfonate (PEDOT : PSS) that was lithographically patterned to define the anode structure. A blend of poly(3-hexylthiophene) (P3HT) and 1-(3-methoxycarbonyl)-propyl-1-phenyl-(6,6)C₆₁ (PCBM) was then spin-coated from a 1 : 1 mixture by weight of the two components in dichlorobenzene, and the device was completed by vacuum deposition of an aluminium electrode in vacuum. The resulting photodiodes had short-circuit quantum efficiencies of 45% and peak power efficiencies of 3%, which compare favourably with values for similar devices fabricated on rigid indium tin oxide (ITO) coated glass substrates.

Introduction

Semiconducting polymers are of scientific and commercial interest owing to their applications in optoelectronic devices such as light-emitting diodes, solar cells and thin-film transistors.¹ There has been significant progress in the development of polymer devices with, for example, small displays based on polymer light-emitting diodes (LEDs) now entering the market place as viable contenders to LCDs.² The current state-of-the-art devices, however, are fabricated on rigid glass substrates coated with indium tin oxide (ITO), and so do not make full use of the processing advantages of organic materials. In particular, they do not exploit the potential for low-cost large-area reel-to-reel manufacturing, which requires the use of a conformable substrate. Accordingly, in recent years, many researchers have sought to fabricate organic devices on flexible ITO-coated plastic substrates.^{3–6} The use of such substrates, however, presents significant technological challenges because plastics suffer from significant thermal shrinkage and are therefore only suited to low temperature processing routes. ITO by contrast should ideally be deposited and annealed above 350 °C to achieve optimal film quality.⁷ The deposition of ITO on plastic substrates must be carried out at significantly lower temperatures resulting in porous films with lower conductivity, reduced transparency and poorer substrate-adhesion, which leads ultimately to reduced device quality.⁷ The SUMITOMO Bakelite Co. Ltd for instance sell ITO-coated polyethyleneterephthalate (PET) foils (FST-1773) with a surface resistivity of 280 Ω/sq. which compares with less than 10 Ω/sq. for good quality ITO-coated glass.

These issues, together with the tendency of ITO to crack when the substrate is bent, have led researchers to seek alternative anode materials for flexible applications. A variety

of materials systems have been proposed including other metal-oxides,⁸ thin metallic films,⁹ polymer–metal composites;⁷ polymer–fullerene composites,¹⁰ and conducting polymers.^{11–16} Conducting polymers are especially appealing because they can be deposited over large areas using techniques such as blade-coating, and planographic or inkjet printing, with obvious potential for reel-to-reel implementation. There are still considerable issues to be addressed before conducting polymers become a suitable replacement for ITO—most notably the need for improved transparency and conductivity—but materials such as polyaniline and poly(3,4-ethylene-dioxythiophene):polystyrene sulfonate (PEDOT : PSS) already show considerable promise as polymeric anodes.^{11–16} In recent work,¹⁷ for example, we fabricated polymer LEDs on flexible PET substrates using PEDOT : PSS as the anode, a blend of poly(9,9-dioctylfluorene-co-benzothiadiazole) and poly(9,9-dioctylfluorene-co-N-(4-butyl-phenyl)di-phenyl-amine) as the emissive layer, and LiF/Al as the cathode. The devices had high peak efficiencies of 13.7 lm W⁻¹ and 8.8 cd A⁻¹, which compared well with the efficiencies of similar devices fabricated on ITO-coated glass substrates.

In this work we evaluate the performance characteristics of photodiodes with PEDOT : PSS anodes against those of comparable devices with standard ITO-coated glass anodes. The provision of high quality polymer photodiodes on flexible substrates offers the possibility for low cost reel-to-reel manufacturing of solar cells, imaging equipment, and optical sensors. In this paper, we are primarily concerned with these latter two applications, and hence focus our attention on the performance of the organic devices under low intensity illumination.

Experimental

Our flexible PET substrates were commercially sourced 100 μm overhead projector sheets, and the anode patterns were lithographically defined in a 120 nm layer of Baytron P (a high conductivity formulation of PEDOT : PSS from

^a Experimental Solid State Physics Group, The Blackett Laboratory, Imperial College London, UK SW7 2AZ. E-mail: a.bradley@imperial.ac.uk

^b Electronic Materials Group, Department of Chemistry, Imperial College London, UK SW7 2AZ. E-mail: j.demello@imperial.ac.uk

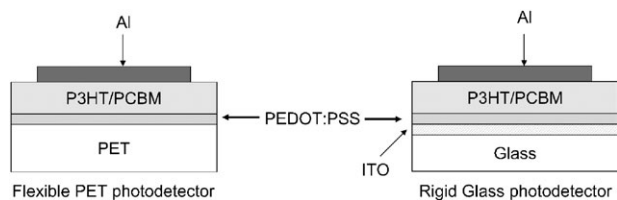


Fig. 1 Schematic diagrams of the flexible PET and rigid glass devices. The anode for the flexible device comprises a 120 nm layer of PEDOT:PSS coated directly on top of the PET substrate. The rigid device uses a 120 nm layer of PEDOT:PSS on 10 Ω /sq. ITO-coated glass. The remaining layers are identical for the two devices: the active layer was a 90 nm 1 : 1 blend of poly(3-hexylthiophene) (P3HT) and 1-(3-methoxycarbonyl)-propyl-1-phenyl-(6,6)C61 (PCBM) and the cathode was 100 nm of thermally deposited Al.

H.C. Starck GmbH). The PEDOT:PSS coated substrate was annealed at 120 °C for 20 min in a dry nitrogen atmosphere to remove trapped water, which is known to reduce the PEDOT:PSS conductivity.¹⁸ A 90 nm active layer of poly(3-hexylthiophene) (P3HT) and 1-(3-methoxycarbonyl)-propyl-1-phenyl-(6,6)C61 (PCBM) was then deposited from a 1 : 1 blend by weight of the two components in dichlorobenzene. Finally, 100 nm of aluminium was deposited through a shadow mask onto the polymer film in vacuum (2×10^{-6} Torr). The pixel area, defined by the overlap of the anode and cathode, was ~ 1.5 mm². The completed devices were thermally annealed at 120 °C in nitrogen for 30 min prior to use. For purposes of comparison, rigid devices of similar structure were fabricated using ITO-coated glass substrates. The remaining layers were the same as for the flexible device, namely: Baytron P (120 nm)/P3HT:PCBM (90 nm)/Al (100 nm). The structures of the flexible and rigid devices are shown in Fig. 1.

The photocurrent action spectra of the polymer devices were determined using a 150 W xenon lamp (Bentham Instruments Ltd, Reading, UK), a CM110 monochromator (CVI Technical Optics, Onchan, UK), and a 236 Source-Measure-Unit [SMU] (Keithley, USA). The action spectra were corrected for the intensity of incident light, using a reference spectrum measured with a calibrated silicon photodiode (UV-818, Newport, UK). The current–voltage characteristics were measured using the 555 nm output of the monochromator, at which wavelength the incident optical power was determined to be 0.26 μ W. All measurements were carried out in a sealed nitrogen environment at room temperature.

Results and discussion

Fig. 2 shows action spectra for the flexible PET (dashed line) and rigid glass (solid line) devices. The two devices have essentially identical spectral characteristics, exhibiting a broadband photoresponse below ~ 675 nm and similar peak quantum efficiencies η_{\max} of 45 and 50%, respectively, at 475 nm. These are relatively high values that compare reasonably with peak quantum efficiencies of $\sim 70\%$ reported by Kim *et al.* for state-of-the-art rigid glass devices based on P3HT/PCBM.¹⁹ (The somewhat lower efficiency of our devices compared with those of Kim *et al.* is due to the use here of a thinner active layer, 90 nm *versus* 175 nm). Importantly, the

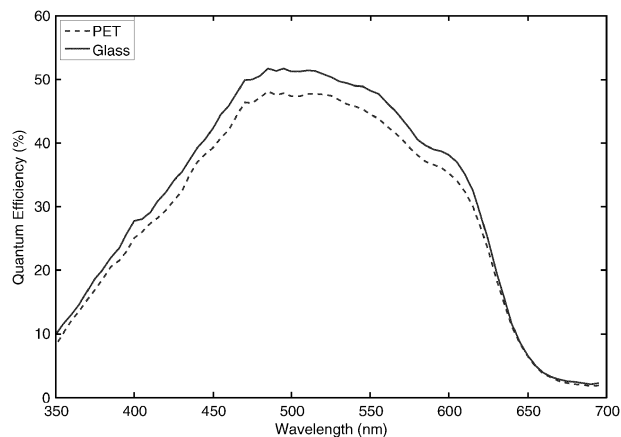


Fig. 2 The photocurrent action spectra for typical flexible PET and rigid glass devices. The action spectra are essentially identical, although the peak quantum efficiencies of the rigid glass devices ($\sim 50\%$) tend to be slightly higher on average than those of the flexible PET devices ($\sim 45\%$).

PET devices are highly flexible and continue to function without any obvious problems, even when rolled up tightly (radius, $r_B < 4$ mm).

Typical IV characteristics in the dark and under 0.26 μ W 555 nm illumination are shown in Fig. 3. The short-circuit dark currents j_0 for the selected pixels were 2.23×10^{-6} A m⁻² for the PET device and 1.49×10^{-6} A m⁻² for the glass device. These low currents indicate a relatively low density of conductive shunts within the devices. In principle, the current density should be zero at short-circuit (since the device is in equilibrium), but in reality the power supply used to bias the device applies a small non-zero voltage δV of ~ 1 mV even when nominally set to zero, causing a small non-zero current to flow through any shunts that are present in the devices. In the context of unbiased photodetectors, if e is the electronic charge and η is the quantum efficiency, then the ratio $j_0/\eta e$

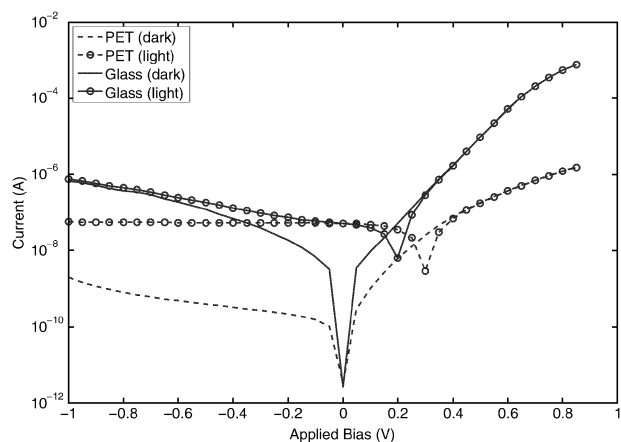


Fig. 3 The current–voltage characteristics for typical flexible PET and rigid glass devices. The rigid glass devices tend to have significantly higher dark currents due to the base-layer of ITO underneath the PEDOT:PSS. The open-circuit voltage of the (illuminated) glass device is lower than that of the (illuminated) PET device due to the higher dark current.

represents the minimum detectable photon flux \mathfrak{I}_0 (*i.e.* it represents a background signal beneath which it is difficult to detect a photo-current). This yields values of $\mathfrak{I}_0 \sim 3 \times 10^{13} \text{ m}^{-2}$ and $\mathfrak{I}_0 \sim 2 \times 10^{13} \text{ m}^{-2}$ for the PET and glass devices, respectively. The dark current j_D under both forward and reverse bias is much higher for the glass device, and the rectification ratio is significantly lower. (A low dark current and a high rectification ratio are desirable for devices operating under reverse biased conditions and, in this respect, the PET devices are preferable to the glass ones.)

The short-circuit photocurrent $j_{\text{photo}}(0)$ under 0.26 μW 555 nm illumination was $\sim 3.3 \times 10^{-2} \text{ A m}^{-2}$ for the two devices, indicating identical short-circuit quantum efficiencies of 43% for the pixels selected. (Note, these were different pixels than those used for the data in Fig. 2.) The open-circuit voltages were 0.33 and 0.19 V for the PET and glass devices, respectively. The lower open-circuit voltage of the ITO-containing device is directly attributable to the higher dark current. The open-circuit voltage corresponds to the voltage at which the total current is zero, *i.e.* it corresponds to the voltage at which the negative photo-current $j_{\text{photo}}(V)$ due to the incident light is balanced exactly by the positive injection-current $j_{\text{injection}}(V)$ due to the potential difference across the electrodes. The injection current is equal to the measured dark current $j_{\text{dark}}(V)$ which, in the case of the two devices considered here, is much higher for the ITO device. The rigid ITO device accordingly has the lower open-circuit voltage.

The higher dark-current (and the lower corresponding open-circuit voltage) in the ITO device has a somewhat surprising consequence: at the low illumination levels considered here, the peak power efficiency of the PET device is actually higher than that of the glass device. The power P dissipated in the photodiode at a voltage V is given by $P = VI$ where I is the current. The operating range of a solar cell corresponds to the voltage range $0 < V < V_{\text{OC}}$ since, in this range, P is negative and the solar cell therefore dissipates energy to the external circuit. In Fig. 4 we show the power dissipation curves for the two devices. Although the voltage resolution is fairly coarse, it is clear that the peak output power is substantially higher for the PET device: $\sim 7 \text{ nW}$ versus $\sim 5 \text{ nW}$ which, expressed as a percentage of the incident

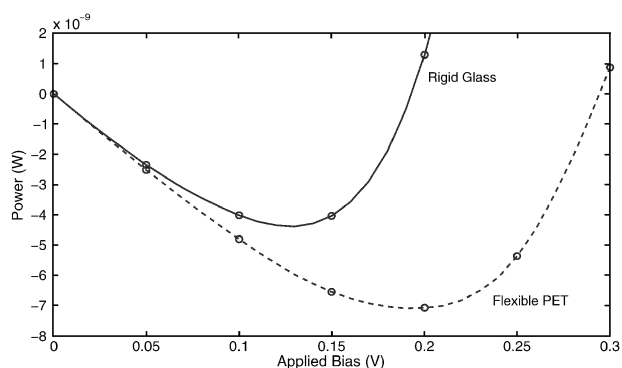


Fig. 4 The power–voltage characteristics for the flexible PET and rigid glass devices shown in Fig. 3. The peak power efficiency of the PET device ($\sim 3\%$) is higher than that of the glass device (2%) due to the higher open-circuit voltage.

optical power, equates to 3% versus 2%. The points of optimal power dissipation are obtained at approximately 0.2 and 0.125 V for the PET and glass devices, corresponding to respective load resistances of $(0.2^2/7 \times 10^{-9}) \sim 5.7 \text{ M}\Omega$ and $(0.125^2/5 \times 10^{-9}) \sim 3.1 \text{ M}\Omega$.

As noted above, the dark current is significantly higher for the rigid device, and it is important to determine whether this is simply because the high conductivity ITO base-layer lowers the series resistance of the rigid device or whether the ITO has a more complicated influence on device operation. In order to obtain further insight into the device operation, it is useful to investigate how, for the two devices, the photo-current $j_{\text{photo}}(V)$ varies with the internal field in the semiconductor. As noted above, the total current under illumination, $j_{\text{total}}(V)$, is equal to the sum of the photocurrent and the dark current:

$$j_{\text{total}}(V) = j_{\text{photo}}(V) + j_{\text{dark}}(V). \quad (1)$$

$j_{\text{photo}}(V)$ can therefore be obtained by subtracting the dark current from the total current, and the resultant curves for the rigid and flexible devices are shown in Fig. 5. The two curves decrease monotonically in magnitude from 10^{-2} A m^{-2} at $V = 0$ (due to their identical short circuit quantum efficiencies) to zero at $V = 0.45 \text{ V}$. In between these limits, however, the magnitude of j_{photo} is consistently lower for the flexible device than for the rigid device. It is interesting to enquire whether this difference can be attributed to the higher conductivity of the ITO base-layer in the rigid device.

The photodiode may be represented conceptually by the equivalent circuit in Fig. 6, in which the current source represents j_{photo} , the diode and shunt resistance account for j_{dark} , and R_S corresponds to the series resistance of the electrodes. The operating voltage, *i.e.* the potential difference across the load resistance R_L , is denoted V and the potential difference across the photo-active layer is denoted V' . R_S and R_L act as a potential divider for the voltage V' so V and V' are related by the expression

$$\frac{V}{V'} = \frac{R_L}{R_L + R_S} \quad (2)$$

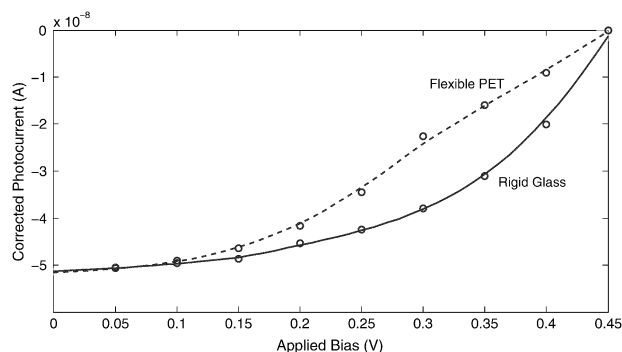


Fig. 5 The corrected-photocurrent versus voltage characteristics for the flexible PET and rigid glass devices shown in Fig. 3. The corrected photocurrent, $j_{\text{photo}}(V)$, is obtained by subtracting the dark current from the current measured under illumination. The magnitude of the corrected-photocurrent is smaller for the PET device due to the higher series resistance.

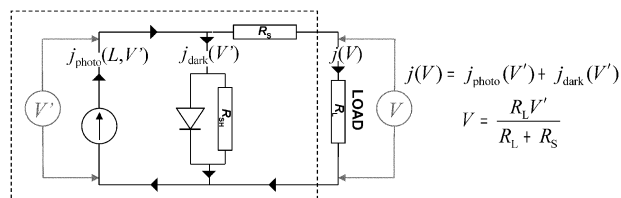


Fig. 6 An equivalent circuit diagram for the photodiodes. See main text for further details.

The electric field inside the photo-active layer is given by $E = (V' - V_{\text{BI}})/d$ where V_{BI} is the built-in potential and d is the thickness of the active layer. From eqn (2) E can be written in the form:

$$E = (V - V_{\text{BI}})/d + R_S V / R_L d \quad (3a)$$

or

$$E = E_0 + R_S V / R_L d \quad (3b)$$

where $E_0 = (V - V_{\text{BI}})/d$ is the field that would be obtained in the ideal situation that the electrodes have zero series resistance ($R_S = 0$). Hence, remembering that the internal field is negative and that the operating voltage V is positive, the overall effect of the series resistance is to decrease the magnitude of the internal field by an amount $R_S V / R_L d$ relative to the $R_S = 0$ situation.

The internal field plays an important role in the generation of the photocurrent, since it promotes exciton dissociation and helps to drive the photogenerated electrons and holes to their respective electrodes, thereby reducing the probability of electron-hole recombination in the bulk. In consequence, j_{photo} is expected to decrease monotonically with operating voltage from a maximum value of j_{SC} at $V = 0$ (when the internal field is largest) to zero at the flat-band voltage (when there is no driving force for charge separation).

In between these two extremes, the effect of the series resistance of the electrode is to reduce the magnitude of the internal field from E_0 to the smaller (negative) value $E_0 + R_S V / R_L d$. Hence, the higher value of j_{photo} in the case of the rigid device is indeed consistent with the lower series resistance of the ITO/PEDOT:PSS anode.

One factor that is difficult to rationalise, however, is the coincidence of the flat-band voltages for the two devices. The flat-band voltage corresponds to $V' = V_{\text{BI}}$ and therefore from eqn (2) is expected to occur at a voltage

$$V_{\text{flat-band}} = \frac{R_L V_{\text{BI}}}{R_L + R_S} \quad (4)$$

If the conductivity of the PEDOT:PSS is sufficiently high then the work function of the PEDOT:PSS-coated ITO anode should be equal to that of the PEDOT:PSS (*i.e.* the contact potential between the ITO and the PEDOT:PSS should appear at the ITO/PEDOT:PSS interface). If this is the case then the built-in potential should be the same for the two devices and hence, from eqn (4), the flat-band voltage should be lower for the flexible device due to the higher series resistance. The fact that this is not the case suggests that the ITO does not merely serve as a high conductivity base-layer

for the rigid device but actually affects the device operation in a more complex manner. Further investigations are currently underway to clarify this.

Conclusion

In summary, we have reported the characteristics of flexible P3HT/PCBM polymer photodiodes on PET substrates with anodes comprising a layer of the conducting polymer PEDOT:PSS. These devices have quantum efficiencies of 45% and power efficiencies of 3% under weak illumination conditions, which compare very favourably to similar devices on ITO-coated glass substrates. The suitability of these devices for solar power generation is not yet known since the measurements were only performed at low illumination levels, and further investigations are therefore required to determine whether the flexible devices remain competitive with the rigid devices at solar illumination levels (AM1.5). In the case of high-sensitivity photodetection, however, it is the performance of the devices under low illumination levels that is relevant, *i.e.* the ability of the devices to detect low photon fluxes. In this regard, the flexible devices compare extremely favourably with standard ITO devices, showing similar quantum efficiencies (45% for the flexible device *versus* ~50% for the rigid devices) and similar (very low) dark currents ($2.23 \times 10^{-6} \text{ A m}^{-2}$ *versus* $1.49 \times 10^{-6} \text{ A m}^{-2}$). These values together imply minimum detectable photon fluxes of $\mathfrak{F}_0 \sim 3 \times 10^{13}$ and $\mathfrak{F}_0 \sim 2 \times 10^{13} \text{ m}^{-2}$ for the PET and glass devices, respectively, and indicate that the flexible devices can be used for a range of applications requiring high sensitivity detection.

Acknowledgements

We would like to thank Dr Jenny Nelson for helpful discussions, Merck Chemicals Ltd for providing the P3HT polymers used in this study, and the UK Engineering and Physical Sciences Research Council (GR/R58949/01) for financial support.

References

- J. M. Shaw and P. F. Seidler, *IBM J. Res. Dev.*, 2001, **45**, 3.
- News release: *Cambridge Display Technology receives first order for PLED display products*. 14 March 2003. http://www.cdtltd.co.uk/press/archive_press_release_index/2003/99.asp.
- M. A. De Paoli, A. F. Nogueira, D. A. Machado and C. Longo, *Electrochim. Acta*, 2001, **46**, 4243.
- F. Padinger, R. S. Tittberger and N. S. Sariciftci, *Adv. Funct. Mater.*, 2003, **13**, 85.
- M. Al-Ibrahim, H. K. Roth and S. Sensfuss, *Appl. Phys. Lett.*, 2004, **85**, 1481.
- M. Al-Ibrahim, H. K. Roth, U. Zhokhavets, G. Gobsch and S. Sensfuss, *Sol. Energy Mater. Sol. Cells*, 2005, **85**, 13.
- K. Yamada, K. Tamano, T. Mori, T. Mizutani and M. Sugiyama, *Proceedings of the 7th international Conference on Properties and Applications of Dielectric Materials*, IEEE Dielectrics and Electrical Insulation Society, Denki Gakkai, Nagoya, Japan, 2003, p. 49.
- J. J. Ho, *Electron. Lett.*, 2003, **39**, 458.
- J. Lewis, S. Grego, B. Chalamala, E. Vick and D. Temple, *Appl. Phys. Lett.*, 2004, **85**, 3450.
- J. S. Moon, J. H. Park, T. Y. Lee, J. B. Yoo, C. Y. Park and J. M. Kim, *Sixth International Conference on the Science and Application of Nanotubes*, Sweden, 2005, abstract p. 214.

- 11 G. Gustafsson, Y. Cao, G. M. Treacy, F. Klavetter, N. Colaneri and A. J. Heeger, *Nature*, 1992, **357**, 477.
- 12 A. N. Krasnov, *Appl. Phys. Lett.*, 2002, **80**, 3853.
- 13 J. Ouyang, C. Chu, F. Chen, Q. Xu and Y. Yang, *Adv. Funct. Mater.*, 2005, **15**, 203.
- 14 F. Zhang, M. Johansson, M. R. Andersson, J. C. Hummelen and O. Inganäs, *Adv. Mater.*, 2002, **14**, 662.
- 15 V. K. Basavaraj, A. G. Manoj and K. S. Narayan, *IEE Proc. Circuits Devices Syst.*, 2003, **150**, 552.
- 16 G. P. Kushto, W. Kim and Z. H. Kafafi, *Appl. Phys. Lett.*, 2005, **86**, 093502.
- 17 J. Huang, X. Wang, A. J. deMello, J. C. deMello and D. D. C. Bradley, *Appl. Phys. Lett.*, submitted.
- 18 J. Huang, P. F. Miller, J. S. Wilson, A. J. de Mello, J. C. de Mello and D. D. C. Bradley, *Adv. Funct. Mater.*, 2005, **2**, 290.
- 19 Y. Kim, S. Cook, S. M. Tuladhar, S. A. Choulis, J. Nelson, J. R. Durrant, D. D. C. Bradley, M. Giles, I. McCulloch, C. Ha and M. Ree, *Nat. Mater.*, 2006, **5**, 197.